*Biogeochemistry* **70:** 427–445, 2004.


# Comparative endoscopic and SEM analyses and imaging for biofilm growth on porous quartz sand

JIIN-SHUH JEAN[1,*], CHUN-WEN TSAO[2] and MENG-CHEN CHUNG[3]

*[1]Curriculum in Department of Earth Sciences, National Cheng Kung University, Tainan City 701, Taiwan; [2]Current address: Department of Environmental Engineering, Kun Shan University of Technology, Yun Kan, Tainan County 710, Taiwan; [3]Transworld Institute of Technology, Touliu, Yunlin County 640, Taiwan; *Author for correspondence (e-mail: jiinshuh@mail.ncku.edu.tw; phone: +886-6-275-7575 ext 65426; fax: +886-6-274-0285)*

Received 6 December 2003; accepted in revised form 7 May 2004

**Key words:** Endoscope, SEM, Image analysis, Biofilm growth, Thickness variability

**Abstract.** The paper presents an endoscope technique to provide a non-destructive detection and imaging of biofilms on porous sand grains without disturbing the system. This *in situ* observation of biofilm growth was carried out by inserting an endoscope into the reactor after introducing the substrate into a water-saturated quartz sand-packed reactor. As the microbes grew on the media surface with time, an expansion was presented in biofilm area. In this way, the growth of biofilm on porous sand grains could be continuously captured. The expanding of the biofilm image was observed, and the biofilm on the sand grains was measured by image analysis of biofilm cross-sections. In order to further identify the biofilm growth, at the end of experiment the packed reactor was dismantled and biofilms along with the aquifer material were sampled for the biofilm growth observation by the scanning electron microscopy (SEM). The biofilm thickness was also measured by image analysis of biofilm cross-sections. The results demonstrated significant spatial variations in mean biofilm thickness (106.2 ± 12.54 $\mu$m to 243.5 ± 26.53 $\mu$m) and thickness variability (0.07–0.12) using image analysis of SEM. However, the mean biofilm thickness measurements done by image analysis of SEM were about 60–82% smaller compared with those by image analysis of endoscopy. This is because of the dehydration and alteration of the biofilm material after dismantling the reactor for SEM observations. In comparison, we found that the endoscope image could provide a first-hand observation of biofilm growth without disrupting the system, while the SEM image could give a better resolution.

## Introduction

The successful bioremediation of organic contaminants in the environment is usually relevant to the fate of the organic contaminants in the environment and their availability to the degradability of microorganisms. Laboratory simulation of the behavior of microorganisms in the subsurface is a challenging problem. First, the metabolic activities of the microorganisms in the simulated system are usually different from the subsurface environment. These could be caused by the deficiency of oxygen, nutrients or contaminants themselves. Second, any detection of the biomass from the stimulated system could not represent the real amount of biomass in the field. When microbes exist in

subsurface porous media, they will attach to the media and grow as biofilm. The biofilm is assumed to be composed of a continuous film, completely covering the surface of the solid particles. This biofilm includes bacterial cells along with their associated glycocalyx (polysaccharide–protein substances) and various kinds of metabolic by-products (Baveye and Valochhi 1989). A biofilm can produce an extracellular polymeric substance (i.e., alginate) (Vogt et al. 2000).

In porous media, biofilm thickness, hydraulic conductivity, pore velocity distribution, and surface roughness can affect the transport of nutrients and substrates to the growing cells (Cunningham et al. 1991), and, of course, to the rate of bioremediation. Variable biofilm thickness is emerging as a potentially important aspect of biofilm function (Stewart et al. 1993; Murga et al. 1995; de Rosa et al. 1998).

The techniques so far used for measuring variable biofilm thickness are light microscopy (Bryers and Characklis 1981; Trulear and Characklis 1982; Robinson et al. 1984; Zahid and Ganczarczyk 1990; Gjaltema et al. 1994), scanning (Mack et al. 1975; Eighmy et al. 1983; Robinson et al. 1984; LeChevallier et al. 1987; Switzenbaum and Eimstad 1987; Capdeville and Nguyen 1990) and transmission (Mack et al. 1975; Robinson et al. 1984; Christensen et al. 1988; Drury et al. 1993; Murga et al. 1995) electron microscopy, atomic force microscopy (Bremer et al. 1992; Razatos et al. 1998), confocal scanning laser microscopy (Lawrence et al. 1991; Lappin-Scott et al. 1992; de Beer et al. 1994a, b), and Fourier transform infrared spectroscopy (de Beer et al. 1994b). The thickness of biofilm can be measured by image analysis software. However, these methods all require a laborious sampling of biofilms along with the media material, and maintaining the integrity of porous media becomes difficult. Nuclear magnetic resonance imaging (NMRI) techniques for biofilm growth assessment were employed at several works (Lewandowski et al. 1992, 1993, 1994, 1995; Potter et al. 1996; Hoskins et al. 1999). Although NMRI techniques provide a non-destructive method of assessing biofilm growth in porous media (Hoskins et al. 1999), the techniques cannot prevent a high cost for experimental works.

Many studies have mentioned the observation of biofilm in their system. However, the sampling process no longer maintains the integrity of porous media. Here, we present a technique to perform an observation for the biofilm growth after biodegradation of organic contaminants (i.e., benzene, toluene, and xylenes) in porous quartz media in a simulated reactor. This technique provides a non-destructive detection and imaging of biofilms. By using an endoscope connected with a computing image analysis system, the observations and measurements for continuous growth of biofilm in a water-saturated quartz sand-packed reactor can be easily achieved. Generally, the captured image from endoscopy is transformed by the image analysis software to a different gray scale image, and can be further compared with the background. The converted image can then be analyzed for the area of interest. It is no longer necessary to disrupt the system for biofilm samples, which can cause significant detection errors. Therefore, the integrity of porous media can be

maintained in the reactor. In addition, the endoscopic technique is much cheaper and easier in experimental works in contrast to the NMRI technique.

## Materials and methods

### *Reactor design*

A continuous flow in a quartz sand-packed reactor was used for biofilm growth. This glass-made reactor is 24 cm in length and 4 cm in diameter with five observation wells per side. These wells were designed for a non-destructive observation of biofilm growth by using an endoscopic instrument. The observation wells are 1.5 cm in inner diameter and 2.5 cm in height and the distance between each well is about 4 cm. The reactor was set up horizontally and the observation wells vertically, as shown in Figure 1. A portable mini-pump (FMI Mode QV-1) was used for fluids recycling throughout the system, set at a flow rate of 16 ml $min^{-1}$. The outlet was connected to a 2-liter Erlenmeyer flask which served as a medium reservoir. The medium was driven back to the reactor through the pump for circulation. A 16-gauge syringe was

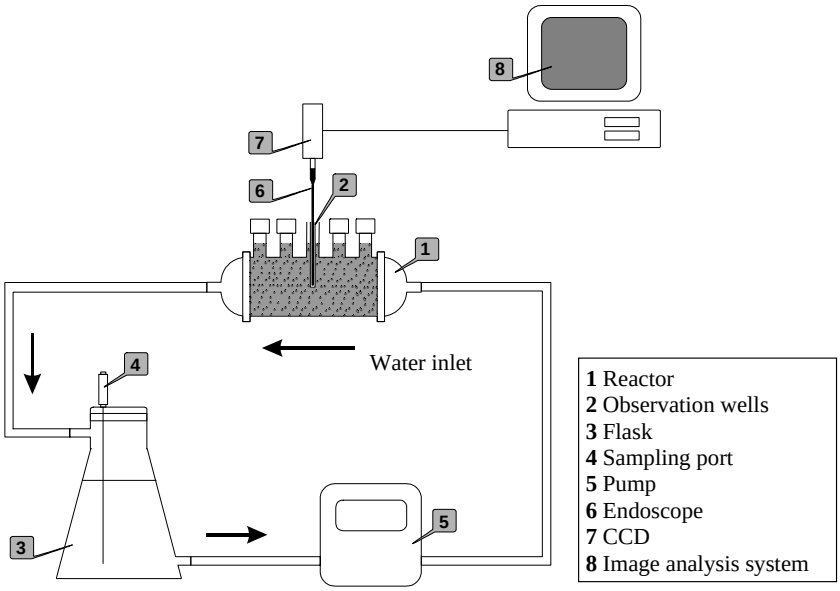


*Figure 1.* The reactor system includes a five-observation-well glass cylinder filled with quartz sand, a portable mini-pump for recycling fluids throughout the whole system, and a sealed flask for effluent storage. The image analysis system, used to capture and store photomicrographic images of biofilm, consisted of a color CCD digital camera mounted on an Olympus industrial endoscope, and image analysis software. Arrows indicate the direction of flow.

used to penetrate the cork for carbon source and mineral salt medium feedings. The reactor system was steadily recycled and hermetically sealed in order to prevent any leaking. The cellulose-nitrate filter membrane with 0.45 $\mu$m pore size was placed at each end of the reactor to stop the discharging of microorganisms. An Erlenmeyer flask was sealed with a silicone cork and Teflon tape to prevent the loss of volatile carbon source.

*The porous media*

The Ottawa quartz sand grains ($\sim$1 mm in diameter), which might be aggregated, were soaked in water until the grains segregated into individuals, and the reactor was subsequently filled in order to enhance the uniform distribution of pores. The water-saturated quartz sands were packed throughout the reactor. A total of 420 g of the treated quartz sands was used to pack the reactor. The quartz sand consisted of $>95\%$ quartz and $<5\%$ iron with the size of 1 mm in diameter, the hardness of 7, and the specific gravity of 2.65. The quartz sand contained negligible amount of organic materials, and was additionally treated at 450 °C oven for 24 h to eliminate any interaction between the organic materials and added substrates.

*The substrates*

A mixture of benzene, toluene, and xylenes compounds (as BTX) in 1:1:1 by volume was injected into the reactor as substrates (carbon source) for bacterial culture. The initial concentration of BTX in the reactor was 17 mg $l^{-1}$. The contents of benzene (Ishizu Seiyaku Ltd., Japan), toluene (Ajax Chemicals, Australia), and xylene polymers (with *ortho*-, *para*-, and *meta*-xylenes, Ajax Chemicals, Australia) used in experiments were all $>99\%$ (v/v).

*The microorganism*

The bacteria taken from the primary sewage treatment plant of the China Petroleum Refinery in Kaohsiung, southern Taiwan, were cultured in BTX mixtures (1:1:1 by volume) and mineral salt nutrients. The procedure for enrichment was performed by adding 1 ml of primary sewage and 99 ml of mineral salt medium into 1 liter of flask. The mineral salt medium, with a pH of 7.0, consisted 5.37 g of $Na_2HPO_4$, 1.36 g of $KH_2PO_4$, 0.5 g of $NH_4Cl$, 0.2 g of $MgSO_4 \cdot 7H_2O$, and 0.02 g of $FeSO_4$ in 1 liter of deionized water. The culture solution was shaken continuously at 150 rpm in a rotary shaker at room temperature ($\sim$25 °C) under aerobic conditions and the substrates (BTX mixtures) were added periodically until the fluid turned turbid and yellowish-brown. After centrifugation, the cell pellet was re-suspended in the mineral

medium. Equal amounts of the bacterial fluids (2 ml per well) were then added to the reactor through the five observation wells (Figure 1).

The bacterial concentration (count) was determined by the pour-plate technique. The initial cell concentration before inoculation was $8.53 \times 10^8$ cells $ml^{-1}$. The bacteria were identified as *Pseudomonas* spp. by Biolog Identification System with more than 90% probability. During the experiment, the samples were withdrawn for bacterial concentration measurements from the observation wells with syringes (Figure 1). The total amount of bacteria determined from five observation wells was added near $8.53 \times 10^8$ cells $ml^{-1}$ which was identical to the initial bacterial concentration injected to the reactor. The BTX mixtures in 1:1:1 by volume were continuously supplied with 50 $\mu$l every day for 7 months. Mineral salt nutrients were supplied at regular intervals. Pure oxygen was aerated through the sampling port when the dissolved oxygen fell below 2 mg $l^{-1}$. These procedures enhanced a ready biodegradation of BTX compounds by bacterial cells, and thus facilitated the growth of biofilms. Measurement of BTX concentrations after biodegradation was not required because of the daily supply and a good re-circulation throughout the system was maintained during the entire experiment period.

### *Endoscopic image analysis system*

To evaluate a non-destructive system, an endoscope was used for image observation through the observation wells of the quartz sand-packed reactor. Observation of biofilm growth on porous quartz sand can be continuously made at any time by inserting the endoscope into the reactor within which biofilms were grown. A small glass tube (1 cm in diameter) with a flat bottom was placed at each observation well in order to protect the front-end of the endoscope lens from abrasion by quartz sand, and to stabilize sand grains so as to fix the measured position and thus facilitate the subsequent observations of endoscope at the same point while keeping it free from disturbance of displacement of saturated sands.

The schematic diagram in Figure 1 describes the idea of image collection. An image analysis system was used to capture and store photomicrographic images of biofilms. The hardware components consist of an endoscope (Endoscope Series 5, R080-144-090-50, Olympus Optical Co. Ltd., Japan), 1445 mm long (843 mm operation length) and 8.1 mm in outer diameter; a color CCD (Model CC-990, Flovel Co. Ltd., Japan) and a digital camera (XC-711, Sony, Japan) with a resolution of 307 thousand pixels. The camera was mounted on the endoscope and used transmitted light. During observations, circular digital images were brought into focus and captured. Collected images of a size of 640 $\times$ 480 pixels at magnifications of nearly 25$\times$ were saved as TIFF files and analyzed with Matrox Inspector software, version 2.2 (Matrox Electronic Systems Ltd., Canada). The spatial resolution is affected by the wavelength of light. The interference from the reflected light of the glass tube and the quartz

sand did limit the resolution. At such low magnification levels, the bacterial cells were not observable. However, the biofilm thickness was measured by endoscopy in this study. The resolution of thickness measurement was 1 pixel or 10 $\mu$m.

During the course for the observation of biofilm growth, the endoscope was inserted into the small glass tube (1 cm in diameter) to take images from the reactor. Since the inserted glass tube separates the endoscope and the sand grains, the working distance is almost the same as the thickness of the bottom of tube ($\sim$0.5 mm). The observable field is about 6 mm in diameter. According to the manufacture's explanation, the depth of field is 5 mm and is defined as the distance from the nearest object plane to the farthest object plane in acceptable focus. When objects are a considerable distance from the lens, the depth of field is large, but with objects closer to the lens, the depth of field decreases rapidly. The observation was carried out at each observation well of the reactor. After finishing the observation and/or image collection, the endoscope was drawn out immediately for another observation. The stored images can thus be compared during each sampling. This technique allows users to maintain a continuous observation of sample biofilms while allowing the reactor to maintain the integrity of the porous media.

*Image analysis*

Analysis of the captured images was also performed using the Matrox Inspector software. The first step of analysis is to segment a specific region of the gray scale image which is of interest. This is called blob analysis and is a powerful image processing technique included in this software. According to the manufacture's explanation, a blob consists of image pixels connected such that one can travel between any two points in the blob while traveling only over points of the same color. Typically, blobs are extracted from binarized images, but conceptually any type of image can be converted into a blob. Objects of interest in the image are filtered from the gray scale values of the image background. The segmentation mask is automatically performed by the software, but can also be manually defined. In this study, the segmentation was defined automatically.

Basically, the transformed gray scale of image can be compared. The darker color in the scale represents a farther distance from the endoscope lens, the lighter color represents a shorter distance from the lens. Thus, the gray–black color scale can be illustrated as the distance from the lens, and the image can be compared and analyzed. The difference in the gray scale was further transformed into a pixel value. Selected objects can be further analyzed in area integration, perimeter, compactness, and roughness (Matrox Inspector software manual). The captured images are presented in resolution of $640 \times 480$ pixels. In order to return the results in true units, a scaled ruler in mm is included in the image taken with an endoscope and analyzed with Matrox Inspector software for pixel measurement. It is estimated that the pixel measurement for distance

between two points is approximately 10 $\mu$m. After each analysis, the obtained image is multiplied by the pixel unit in order to estimate its size. Thus, the size and the roughness of the biofilm could be estimated.

*Scanning electron microscopy analysis*

For confirmation, a further observation of biofilm growth was carried out using scanning electron microscopy (Hitachi S4100 Field Emission SEM, Japan) after dismantling the packed reactor. Since the biofilm structure was assumed to be uniformly formed throughout the reactor, sand grains were taken closer to the same position as the images taken by endoscopy for biofilm analysis. Our assumption was based on the following: (1) Sand grains of about 1 mm in diameter were uniformly distributed throughout the system; (2) 50$\mu$l of BTX (benzene, toluene, and xylene) mixtures in 1:1:1 by volume were injected daily into the reactor for 7 months; (3) Bacterial fluids with $8.53 \times 10^8$ cells $ml^{-1}$ were injected into the reactor from five observation wells (2 ml per well). Then the bacterial cells at each well with equal concentration might be widespread and uniformly distributed throughout the system. Subsequently, the BTX mixtures were biodegraded to form biofilms; (4) As can be seen in the endoscope images in Figure 2, the biofilm growth expanded with time. Based on the above, we can assume the biofilm structure was uniform in the reactor.

After dismantling the packed reactor, biofilms were carefully detached from the sand media, and was placed on carbon tape which was later stuck on a carbon holder and dried before coated with gold foil. The sample was then ready for SEM observations. Then microimages of the biofilm were photographed and both the thickness and the thickness variability were measured using the Matrox Inspector image analysis system. In addition to the endoscopic image, this software was also used to analyze the SEM images obtained.

## Results and discussion

*Calibration of image analysis*

The curvature of the endoscope lens can result in a slight distortion of object images. It is thus required to quantify this effect on image analysis. The calibration was performed for area and for shape (compactness) measurements by using dark hard objects. Darker materials can reduce the effect of reflection. After the taking of images with the endoscope, the area of the objects (in pixels) was transformed and calculated automatically by Matrox Inspector software. The measured value versus the true area gives a ratio as follows:

$$[\text{measured value}] = 1.0055\ [\text{true area}], \quad r^2 = 0.99. \tag{1}$$

The measured value agreed with the true value (data not shown). The deviation of area measurements was within the range of $\pm 3\%$.

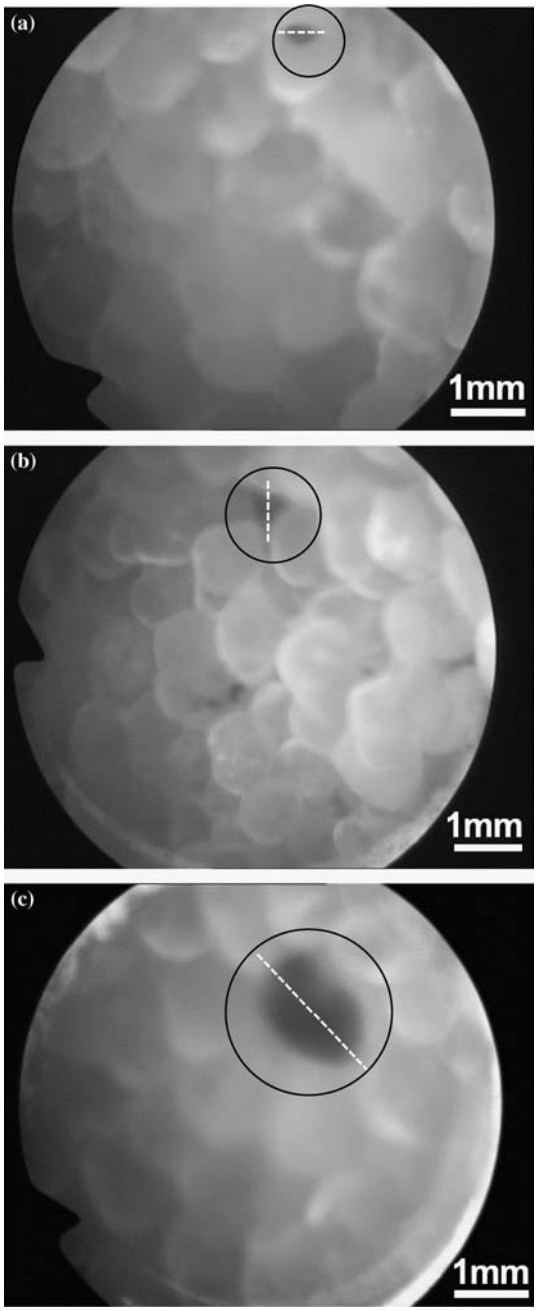
(a)
1mm
(b)
1mm
(c)
1mm

Compactness is a measurement of how close the pixels in the image of the object of interest are to one another. It is a value derived from the perimeter and the area. A circular object is defined to have a compactness of 1.0 (the minimum value) because of its most compact character. The more convoluted the shapes form, the larger the value of compactness is. Circular objects with a theoretical compactness value of unity were used for the calibration. The result revealed that the image taken had a compactness of $1.13 \pm 0.02$ (data not shown) and can be considered circular.

*Observation of biofilm growth*

Measurements of the area are used to present the growth of biofilm. Figure 2 shows three images which were taken by endoscopy at the same well (the middle one in Figure 1) in the fourth, fifth, and the seventh month after the supplement of BTX for biodegradation, as images a, b, and c, respectively. In the images, quartz sand grains of approximately 1 mm in diameter are shown as packed particles, making the biofilm easily observable as the dark area. The circle in Figure 2 indicates the region of biofilm growth and the dark area is the biofilm at a different time. During image taking, packed sand grains sometimes may cause shadows, as in image b. However, the biofilm can be easily distinguished from a thin membrane at the edge of the dark area. The rest of the circle did not observe any biofilm growth in this particular position possibly because the biofilm expanded from the dark area but had not yet exceeded the circle. The reason is that the dark area was around an observation well (Figure 1), where the bacterial fluids were injected into the packed reactor. The expansion in area indicated as the microbes grew on the media surface with time. An increase in area was noticed from $6.07 \times 10^{-2}$ mm$^2$ in the fourth month to 1.389 mm$^2$ in the seventh month (Table 1). This accounts for the biofilm growth by area for 23 times within 4 months. Another observation of biofilm growth with time in the second well (Figure 1) from the water inlet was also presented in Table 1. After 7 months, the biofilm area was $5.41 \times 10^{-1}$ mm$^2$. The area had increased by 18 times within 4 months. However, the growing biofilm seemed not to cover the whole sand grain. The reason could be that the compactness of the sand grains interfered with the biofilm's downward extension, thus the sand grains were not covered as a biofilm grows in an

*Figure 2.* The endoscopic images for biofilm growth on the quartz sand grain at the same location and depth (i.e., the middle observation well in Figure 1) for different times after biodegradation of BTX. (a) 4 months (biofilm area = $6.07 \times 10^{-2}$ mm$^2$); (b) 5 months (biofilm area = $1.19 \times 10^{-1}$ mm$^2$); (c) 7 months (biofilm area = 1.389 mm$^2$). The full field represents the quartz sand grains of approximately 1 mm in diameter. The circle is the region of biofilm growth and the dark area is the biofilm. The rest of the circle did not grow any biofilm. The white dotted line is the linear section for profile analysis of biofilm thickness in Figure 3.

*Table 1.* Endoscopy analyses for the variations in area, compactness, roughness coefficient and thickness of the biofilm growth with time after biodegradation of BTX compounds

| Well | Elapsed time since biodegradation | Area ($mm^2$) | Maximum thickness ($\mu$m) | Mean thickness ($\mu$m) | Compactness | Roughness coefficient | Image |
|---|---|---|---|---|---|---|---|
| Middle | Four months | $6.07\times10^{-2}$ | 444 | 205 | 2.43 | 1.33 | Figure 2a |
| | Five months | $1.19\times 10^{-1}$ | 546 | 189 | 3.36 | 1.53 | Figure 2b |
| | Seven months | 1.389 | 986 | 604 | 3.21 | 1.65 | Figure 2c |
| Second from water inlet | Four months | $2.94\times 10^{-2}$ | 447 | | 2.16 | 1.31 | |
| | Five months | $9.91\times 10^{-2}$ | 537 | | 1.78 | 1.18 | |
| | Seven months | $5.41\times 10^{-1}$ | 974 | | 1.61 | 1.16 | |

ordinary way. The image of scanning electron microscopy (SEM) could support this explanation.

Observation of biofilm shape can be determined by its compactness and roughness coefficient. The compactness of an object is derived from the perimeter and area as described in the last section. A more convoluted shape of biofilm has a higher compactness value (Table 1). The roughness coefficient is a measurement of the unevenness or irregularity of the biofilm surface. Biofilm with many jagged edges has a higher roughness coefficient value. The roughness coefficient increased with time in the middle well, but decreased with time in the second well from the water inlet (Table 1 and Figure 1). This is apparently because the higher flow in the second well from the water inlet could facilitate to wash away the bacterial colonies or biofilms, and thus could limit the formation of the biofilm and decrease the roughness. Therefore, an observation of biofilm growth, in size, area, shape, and location of biofilm, using an endoscope at a certain point could be easily and rapidly detected at any time. The image showed the distributed sand grain in the reactor, and the circle demonstrated the growth of biofilm in different times. However, during the observation, the inserted glass tube was slightly fouled, which affected the resolution as shown in Figure 2. This problem seems to be difficult to avoid and needs to be circumvented in future research.

### *Biofilm thickness*

The thickness of biofilm is also an important aspect of biofilm growth in the porous media. Such measurements were determined from the profile analysis of images using the Matrox Inspector software of the endoscopy and SEM techniques Tables 1 and 2). Captured images were converted to gray-scale TIFF files. The system gives the profile histogram and data with a resolution of 1 pixel or approximately 10 $\mu$m by generating a trace line across the biofilm surface in the image. The thickness of certain point of biofilm matrix can thus be obtained from the difference of the corresponding pixel value and the mean

*Table 2.* Summary statistics for the measurements of biofilm thickness along each of the different sections after seven-months of biofilm growth using SEM image analysis as shown in Figures 4 and 5

| Statistic | a–a′ | b–b′ | c–c′ | d–d′ | e–e′ | f–f′ | g–g′ |
|---|---|---|---|---|---|---|---|
| Measuring points | 208 | 211 | 148 | 201 | 81 | 318 | 197 |
| Mean ($\mu$m) | 227.11 | 211.92 | 231.13 | 243.50 | 106.20 | 134.91 | 122.09 |
| Median ($\mu$m) | 231.07 | 210.98 | 229.19 | 248.65 | 108.86 | 134.14 | 126.86 |
| Minimum ($\mu$m) | 179.58 | 141.91 | 172.05 | 183.35 | 79.71 | 96.00 | 78.86 |
| Maximum ($\mu$m) | 281.30 | 287.58 | 295.12 | 290.09 | 138.00 | 182.57 | 160.29 |
| SD ($\mu$m) | 20.98 | 38.20 | 30.36 | 26.53 | 12.54 | 18.13 | 18.13 |
| Variability[a] | 0.07 | 0.15 | 0.11 | 0.09 | 0.10 | 0.11 | 0.12 |

[a]Calculated from Eq. (2) in this study.

background value (quartz sand in this system). In Table 1, the maximum thickness of the biofilm in the middle well increased from 444 to 986 $\mu$m (122.1% increase) during the fourth to seventh months of elapsed time of biodegradation; in the second well from the water inlet, the increase was from 447 to 974 $\mu$m (117.9% increase). These results show an obvious rise in thickness with biofilm growth.

*Biofilm thickness variability*

Non-uniform distribution of bacterial cells and polymers within the biofilm matrix and variable biofilm thickness gives rise to microscale structural heterogeneities of biofilm (Murga et al. 1995). The spatial variations from the biofilm sections in the endoscopic images are shown in Figure 3 (derived from Figure 2). As previously described in the image analysis, when the gray scale of the sample images is compared and transformed to a pixel value, the thickness of the biofilm can be determined. Although it seems that the images are quantitative, with significant resolution, they were not sufficient to discern the distribution of bacterial cells in biofilms. This problem may be solved by further research to develop an endoscope capable of magnification in the lens in the future. Thus the microscale structural heterogeneity of biofilms could not be determined in the present study.

In order to further identify biofilm thickness variations, we dismantled the reactor and sampled biofilms along with the aquifer material at the end of the experiment. These samples were observed and microphotographed for biofilm growth by SEM. Then the biofilm thickness variations were determined by image analysis of biofilm cross-sections.

The endoscopic image (Figure 2) was observed for biofilm growth in a fixed position, since the lens was inserted into the middle observation well (Figure 1) of the reactor. At the end of experiment (i.e., after 7 months of biofilm growth), we dismantled the reactor and disrupted the sand grains to further identify the biofilm growth using the SEM image, the biofilm samples were collected from the sand grains closer to the same position as the images taken by endoscopy and then photographed by SEM. In Figure 4a, the abundant biofilm was patchy in the center, while other grains did not seem to grow any biofilm. This is possibly because the biofilm expanded from the dark area taken by endoscopy but had not yet exceeded the region of biofilm growth (Figure 2). The dark area was around the middle well (Figure 1) where the bacterial fluids were injected into the packed reactor. With the images of SEM, it shows the shrinkage of biofilm matrix as in Figure 4 possibly caused by the SEM preparation. Spatial variations of biofilm surface were clearly revealed and the variations in thickness were quantified also by using the Matrox Inspector image analysis software. The SEM images were imported into the analysis program and converted to gray scale images. Once the sections were lined and defined on the biofilm surface, the analysis system automatically measured the

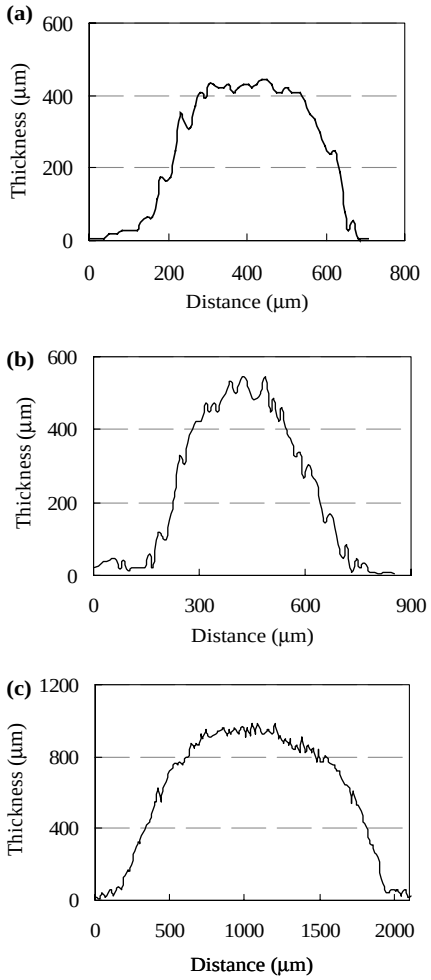


*Figure 3*. The thickness variations of biofilm sections obtained from the endoscopic images for different times after the biodegradation of BTX. (a) After 4 months, corresponding to Figure 2a; (b) after 5 months, corresponding to Figure 2b; (c) after 7 months, corresponding to Figure 2c. Linear sections were profiled across the center of biofilm matrix as the dotted lines in Figure 2.

profile values. The resolution of thickness measurements was 1 pixel or approximately 0.86 $\mu$m. The geometry of the interstices of the aquifer material that microbes attached to and grew on was present as a continuous biofilm, i.e. the biomass phase of continuous biofilm completely covered the surface of sand grain. In the image of Figure 4b, biofilms attached to the sand grain were sloughed off in the center possibly due to the damage either from dismantling the packed reactor or naturally drying. The spatial variations in biofilm thickness versus distance along each section were shown in Figure 5. It is obviously shown that biofilm thickness in different sections of Figure 5 are

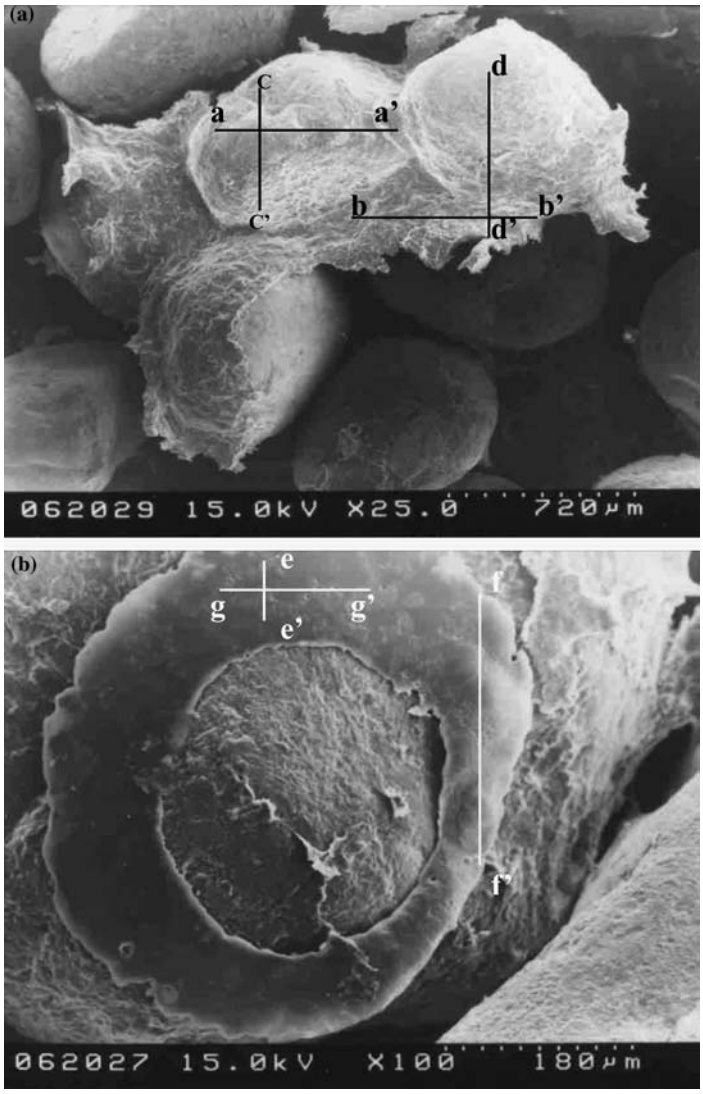


*Figure 4*. Images of biofilms attached to the sand grain taken using scanning electron microscopy (Hitachi S4100 Field Emission SEM, Japan). (a) Biofilms covered completely and continuously among the sand grains at the 7-month growth; (b) biofilms covered the individual grain.

thinner than those of Figure 3 because the biofilm was removed from sand grains and dehydrated for SEM observations.

The substratum where biofilm was grown in this study is composed of quartz sand grains. This is different from that biofilm grown on a stainless-steel slide as reported by Murga et al. (1995) and an electron microscope grid (coated with parlodion) attached to a glass microscope slide as reported by Mack et al.

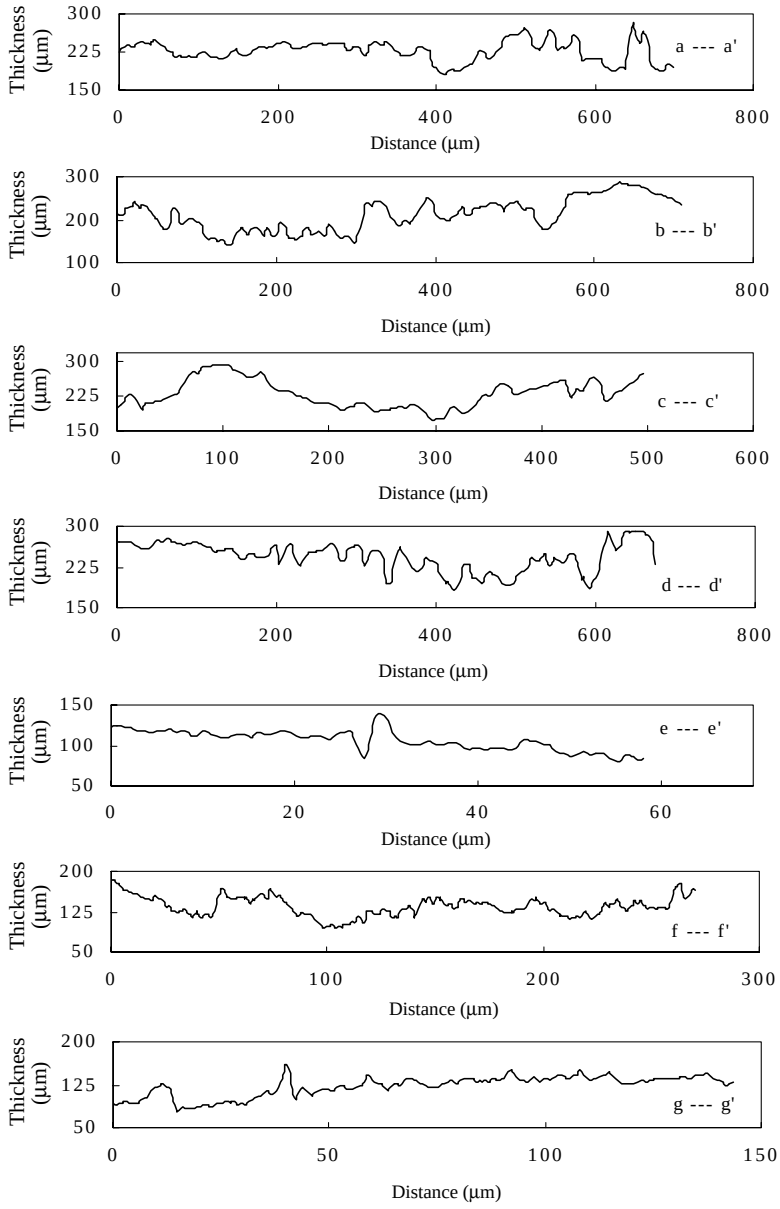


*Figure 5*. Profiles showing spatial variations of biofilm thickness. Sections a–a′, b–b′, c–c′, and d–d′ are lined from the image in Figure 4a and sections e–e′, f–f′, and g–g′ are from Figure 4b.

(1975). After dismantling the studied reactor, the biofilm was carefully detached from the bulk of sand media and placed on carbon tape. This tape was later stuck on a carbon holder and dried before coated with gold foil. The

sample was then ready for the SEM analysis. Then microimages of the biofilm were photographed and both the thickness and the thickness variability were measured using the Matrox Inspector image analysis system. Captured images were then converted to TIFF files. The Matrox Inspector software was used to define the location of the substratum on the computer image by a line and to trace the surface of the biofilm using a mouse (Murga et al. 1995). The system then automatically measured biofilm thickness and the distances between the line and the trace at regular intervals along the substratum. In this study, thickness in Figure 5 was measured every 3.4 $\mu$m for sections a–a′, b–b′, c–c′ and d–d′ and every 1 $\mu$m for sections e–e′, f–f′, and g–g′. The resolution of thickness measurement by SEM was 1 pixel or 0.86 $\mu$m.

Thickness variability, $C_t$, the index of thickness variation relative to the mean thickness, is defined as

$$C_t = \frac{1}{N}\sum_{i=1}^{N}\frac{|T_i - T|}{T} \tag{2}$$

where $T_i$ is the $i$th individual thickness measurement, $T$ is the mean thickness, and $N$ is the number of thickness measurements. The thickness variability over sections a–a′, b–b′, c–c′, d–d′, e–e′, f–f′, and g–g′ (Figures 4 and 5) after 7 months of biofilm growth using SEM image analysis were calculated as 0.07, 0.15, 0.11, 0.09, 0.10, 0.11, 0.12, respectively (Table 2). The mean thickness over the sections ranged from 106.2 ± 12.54 to 243.5 ± 26.53 $\mu$m, which decreased from 604 $\mu$m (60–82% reduction) as computed by endoscopic image analysis. The results demonstrated that the main thickness over measuring points along each of a–a′, b–b′, c–c′, d–d′, e–e′, f–f′, and g–g′ sections varied significantly. Therefore, the results revealed that the biofilm attached to the quartz sand grain demonstrate significant spatial variations in biofilm thickness despite the sand grains (about 1 mm in diameter) being assumed to be uniformly distributed in the packed reactor.

We speculated that this spatial variation was probably caused by the roughness and impurity contents of the sand surface, as well as non-uniform pore distribution. In addition, the dehydration processes in the SEM sample preparation may affect the variation. A comparison of the utilization for sample analysis among endoscope and SEM is summarized in Table 3. The maximum biofilm thickness measured by image analysis of SEM at c–c′ and d–d′ sections in Figures 4a and 5 were 295.1 and 290.1 $\mu$m, respectively. This is about 70% reduction from the 986 $\mu$m endoscopy image analysis. This is caused by the dehydration and alteration of the biofilm material while dismantling the packed reactor for SEM observation. In our study, we found that both techniques have their own advantages and disadvantages. Endoscope images can provide a first-hand observation of biofilm growth without disrupting the system, while the SEM images have a better resolution. However, the image resolution by endoscopy could be improved by using a magnifying lens in the future.

*Table 3*. The comparison of the sample processing and observation between endoscopy and SEM techniques

| | Endoscopy | SEM |
|---|---|---|
| Maximum biofilm thickness ($\mu$m) | 986 | c–c′ section in Figure 5: 295.1 (70% decrease) d–d′ section in Figure 5: 290.1 (70.6% decrease) |
| Disruption of the system for sample analysis | No | Yes |
| Sample damage (dehydration, shrinkage, etc.) | No | Severe |
| *In situ* analysis | Yes | No |
| Trainee experience | Few | Required |
| Cost | Low | High |
| The resolution or signal of the sample image | Poor (10 $\mu$m) but could be improved by using a magnifying lens in the future | Excellent (0.86 $\mu$m) |

The maximum thickness along the cross-sections measured by image analysis of endoscopy (Figures 2c and 3c and Table 1 for the biofilm growth at 7 months in the middle well) and SEM (sections c–c′ and d–d′ in Figures 4a and 5 and Table 2).

## Conclusions

Endoscopic imaging techniques can be used for the non-destructive detection and imaging of biofilms on porous sand grains. The *in situ* observations and measurements for continuous growth of biofilms can be rapidly accomplished using an endoscope without sampling biofilms along with the porous media material, in which the size, area, shape, location, and the thickness of biofilm can be identified with ease. Due to the limitations of low magnification and poor resolution of endoscopy in the present study, image analysis of SEM was used to further identify the biofilm thickness as computed by endoscopy image analysis. However, the biofilm thickness measurement done by image analysis of SEM became thinner than that by endoscopy image analysis. This may result from dehydration and alteration of the biofilm material after disturbing the system for SEM observations. If a magnifying endoscope can be developed in the future, the biofilm thickness and the distribution of bacterial cells in biofilms can also be determined directly from endoscopic images. Thus endoscopic imaging techniques may become a more powerful tool in the *in-situ* observations in many areas.

## Acknowledgments

We thank Chung-Liang Hsieh, Ching-Wen Ko, Yu-Ting Su, and Meng-Huey Chen for their help on adding BTX to the reactor for more than six months and performing the endoscope to obtain images for biofilm growth. This work was funded by the NSC grant 88-2116-M-006-007.

## References


Baveye P. and Valocchi A.J. 1989. An evaluation of mathematical models of the transport of biologically reacting solutes in saturated soils and aquifers. Water Resour. Res. 25: 1413–1421.

Bremer P.J., Geesey G.G. and Drake B. 1992. Atomic force microscopy examination of the topography of a hydrated bacterial biofilm on a copper surface. Curr. Microbiol. 24: 223–230.

Bryers J.D. and Characklis W.G. 1981. Early fouling biofilm formation in a turbulent flow system: overall kinetics. Water Res. 15: 483–491.

Capdeville B. and Nguyen K.M. 1990. Kinetics and modeling of aerobic and anaerobic film growth. Water Sci. Technol. 22: 149–170.

Christensen F.R., Kristensen G.H. and Jansen J. 1988. Biofilm structure: an important and neglected parameter in wastewater treatment water pollution research and control. Water Sci. Technol. 21: 805–814.

Cunningham A.B., Characklis W.G., Abedeen F. and Crawford D. 1991. Influence of biofilm accumulation on porous media hydrodynamics. Environ. Sci. Technol. 25: 1305–1311.

de Beer D., Stoodley P., Roe F. and Lewandowski Z. 1994a. Effects of biofilm structures on oxygen distribution and mass transport. Biotechnol. Bioeng. 43: 1131–1138.

de Beer D., Stoodley P., Roe F. and Lewandowski Z. 1994b. Liquid flow in heterogeneous biofilms. Biotechnol. Bioeng. 44: 636–641.

de Rosa S., Sconza F. and Volterra L. 1998. Biofilm amount estimation by fluorescein diacetate. Water Res. 32: 2621–2626.

Drury W.J., Stewart P.S. and Characklis W.G. 1993. Transport of 1- $\mu$m latex particles in *Pseudomonas aeruginosa* biofilms. Biotechnol. Bioeng. 42: 111–117.

Eighmy T.T., Maratea E. and Bishop P.L. 1983. Electron microscopic examination of wastewater biofilm formation and structural components. Appl. Environ. Microbiol. 45: 1921–1931.

Gjaltema A., Arts P.A.M., van Loosdrecht M.C.M., Kuenen J.G. and Heijnen J.J. 1994. Heterogeneity of biofilms in rotating annular reactors: occurrence, structure and consequences. Biotechnol. Bioeng. 44: 194–204.

Hoskins B.C., Fevang L., Majors P.D., Sharma M.M. and Georgiou G. 1999. Selective imaging of biofilms in porous media by NMR relaxation. J. Magn. Reson. 139: 67–73.

Lappin-Scott H.M., Costerton J.W. and Marrie T.J. 1992. Biofilms and biofouling. In: Lederberg E.J. (ed), Encyclopaedia of Microbiology, Vol. 1. Academic Press, San Diego, pp. 277–284.

Lawrence J.R., Korber D.R., Hoyle B.D., Costerton J.W. and Caldwell D.E. 1991. Optical sectioning of microbial biofilms. J. Bacteriol. 173: 6558–6567.

LeChevallier M.W., Babcock T.M. and Lee R.G. 1987. Examination and characterization of distribution system biofilms. Appl. Environ. Microbiol. 53: 2714–2724.

Lewandowski Z., Altobelli S.A., Majors P.D. and Fukushima E. 1992. NMR imaging of hydrodynamics near microbially colonized surfaces. Water Sci. Technol. 26: 577–584.

Lewandowski Z., Altobelli S.A. and Fukushima E. 1993. NMR and microelectrode studies of hydrodynamics and kinetics in biofilms. Biotechnol. Progr. 9: 40–45.

Lewandowski Z., Stoodley P., Altobelli S. and Fukushima E. 1994. Hydrodynamics and kinetics in biofilm systems: recent advances and new problems. Water Sci. Technol. 29: 223–229.

Lewandowski Z., Stoodley P. and Altobelli S.A. 1995. Experimental and conceptual studies on mass transport in biofilms. Water Sci. Technol. 31: 153–162.

Mack W.N., Mack J.P. and Ackerson A.O. 1975. Microbial film development in a trickling filter. Microb. Ecol. 2: 215–226.

Murga R., Stewart P.S. and Daly D. 1995. Quantitative analysis of biofilm thickness variability. Biotechnol. Bioeng. 45: 503–510.

Potter K., Kleinberg R.L., Brockman F.J. and McFarland E.W. 1996. Assay for bacteria in porous media by diffusion-weighted NMR. J. Magn. Reson. Ser. B 113: 9–15.

Razatos A., Ong Y.L., Sharma M.M. and Georgiou G. 1998. Evaluating the interaction of bacteria with biomaterials using atomic force microscopy. J. Biomater. Sci. (Polymer Ed.) 9: 1361–1373.

Robinson R.W., Akin D.E., Nordstedt R.A., Thomas M.V. and Aldrich H. C. 1984. Light and electron microscopic examinations of methane-producing biofilms from anaerobic fixed-bed reactors. Appl. Environ. Microbiol. 48: 127–136.

Stewart P., Peyton B.M., Drury W.J. and Murga R. 1993. Quantitative observations of heterogeneities in *Pseudomonas aeruginosa* biofilms. Appl. Environ. Microbiol. 9: 327–329.

Switzenbaum M.S. and Eimstad R.B. 1987. Analysis of anaerobic biofilms. Environ. Technol. Lett. 8: 21–32.

Trulear M.G. and Characklis W.G. 1982. Dynamics of biofilm processes. J. Water Pollut. Cont. Fed. 54: 1288–1301.

Vogt M., Flemming H.C. and Veeman W.S. 2000. Diffusion in *Pseudomonas aeruginosa* biofilms: a pulsed field gradient NMR study. J. Bacteriol. 77: 137–146.

Zahid W.M. and Ganczarczyk J.J. 1990. Structure of RBC biofilms. Water Environ. Res. 66: 100–106.